Environ Earth Sci
DOI 10.1007/s12665-010-0488-4

ORIGINAL ARTICLE

Laboratory and numerical modeling of water balance in a layered sloped soil cover with channel flow pathway over mine waste rock

Qing Song · Ernest K. Yanful

Received: 25 September 2009 / Accepted: 5 February 2010

Abstract Macropores developed in barrier layers in soil covers overlying acid-generating waste rock may produce preferential flow through the barrier layers and compromise cover performance. However, little has been published on the effects of preferential flow on water balance in soil covers. In the current study, an inclined, layered soil cover with a 10-cm-wide sand-filled channel pathway in a silty clay barrier layer was built over reactive waste rock in the laboratory. The channel or preferential flow pathway represented the aggregate of cracks or fissures that may occur in the barrier during compaction and/or climate-induced deterioration. Precipitation, runoff, interflow, percolation, and water content were recorded during the test. A commercial software VADOSE/W was used to simulate the measured water balance and to conduct further sensitivity analysis on the effects of the location of the channel and the saturated hydraulic conductivity of the channel material on water balance. The maximum percolation, 80.1% of the total precipitation, was obtained when the distance between the mid-point of the channel pathway and the highest point on the slope accounted for 71% of the total horizontal length of the soil cover. The modeled percolation increased steadily with an increase in the hydraulic conductivity of the channel material. Percolation was found to be sensitive to the location of the channel and the saturated hydraulic conductivity of the channel material, confirming that proper cover design and construction should aim at minimizing the development of vertical preferential flow in barrier layers. The sum of percolation and interflow was relatively constant when the location of the channel changed along the slope, which may be helpful in locating preferential flow pathways and repairing the barrier.

Keywords Acid rock drainage · Channel flow · Laboratory test · Soil cover · VADOSE/W · Water balance

Introduction

Acid rock drainage (ARD) from the oxidation of reactive waste rock is a major concern in the mine industry. Treatment and prevention are considered two important methods for dealing with the problem (Egiebor and Oni 2007). The use of an engineered soil cover incorporating a capillary barrier over the waste rock has been found to be an effective approach to mitigate ARD due to decreased influx of water and gaseous oxygen into the waste rock. A capillary barrier is usually comprised of a layer of coarse-grained material (such as sand or gravel) underlying a layer of fine-grained material. The capillary barrier effect has been extensively studied in the laboratory and at many sites (e.g., Nicholson et al. 1989; Akindunni et al. 1991; Woyshner and Yanful 1995; O'Kane et al. 1998; Choo and Yanful 2000; Bussière et al. 2003; Fala et al. 2005; Adu-Wusu et al. 2007). The moisture distribution in the barrier or fine layer can be influenced by a number of factors including a change in the geometry of the soil cover. For

Electronic supplementary material The online version of this article (doi:10.1007/s12665-010-0488-4) contains supplementary material, which is available to authorized users.

Q. Song (✉) · E. K. Yanful
Geotechnical Research Center,
Department of Civil and Environmental Engineering,
University of Western Ontario, 1151 Richmond Street,
London, ON N6A 5B9, Canada
e-mail: qsong3@uwo.ca

E. K. Yanful
e-mail: eyanful@eng.uwo.ca

Published online: 24 February 2010

example, some of the water available to infiltrate into the barrier layer may be diverted laterally in a sloped cover, resulting in decreased saturation upslope during drying period (Bussière et al. 2003).

Another factor affecting the moisture distribution and the performance of the soil cover is preferential flow in the barrier layer. Macropore flow (Beven and Germann 1982), fingered flow (Hill and Parlange 1972; Selker et al. 1992), and funnel flow (Kung 1990; Walter et al. 2000) are three kinds of preferential flow mechanisms. Among them, macropore flow is the main concern related to soil cover performance because percolation into the underlying waste could increase significantly when macropores occur in the barrier layer. Macropores could develop from a number of mechanisms including plant root penetration, animal intrusion, freeze–thaw, and desiccation (Beven and Germann 1982; Corser and Cranston 1991; Suter et al. 1993). In the field, macropore flow has been found to contribute to the deterioration of soil covers (Taylor et al. 2003; Adu-Wusu and Yanful 2006, 2007). However, soil covers with macropore flow has not been studied systematically in the laboratory under controlled conditions. Such controlled studies are necessary to understand how the resulting preferential flow influences water balance parameters such as interflow, runoff and percolation. Such studies also provide useful data for calibrating computer models.

Laboratory or field calibrated computer models provide cost-effective tools for evaluating and predicting soil cover performance, especially, over the long term, when measured data may not be available. Such combined experimental and modeling approach has been used extensively by many researchers (e.g., Khire et al. 1999; Scanlon et al. 2002; Swanson et al. 2003; Yanful et al. 2003; Bussière et al. 2003; Adu-Wusu et al. 2007). Modeling allows hypothetical cases to be run and re-run to check the sensitivity of certain parameters following calibration of the program. Although a number of computer programs can simulate water flow in soils under saturated–unsaturated conditions, some of them are more commonly used than others for the evaluation of water transfer in soil covers. These programs include one-dimensional (1D) models, such as Soilcover (Wilson et al. 1994), UNSAT-H (Fayer 2000), HYDRUS-1D (Simunek et al. 2005), and two-dimensional (2D) models, such as HELP (Schroeder et al. 1994), HYDRUS-2D (Simunek et al. 1999), SEEP/W (GEO-SLOPE 2002), VADOSE/W (GEO-SLOPE 2004). Recently, 2D models have seen more extensive applications than 1D models because actual soil covers rarely behave as 1D systems (Aubertin and Bussière 2001). VADOSE/W (GEO-SLOPE 2004) is a 2D finite element program that incorporates heat, water vapor, and gas flow in its fundamental equations. The oxygen transfer formulation embedded in the program makes it possible to directly calculate influx of oxygen into the underlying waste rock, which is important in the evaluation of soil cover performance during ARD mitigation. Recently, VADOSE/W has been used successfully to model water balance and oxygen flux in field test plots at Whistle mine site, Ontario, Canada (Adu-Wusu et al. 2007; Song and Yanful 2008).

In the current study, a soil cover consisting of compacted silty clay and construction sand was placed over a waste rock layer with a 20% of slope in the laboratory. A 10-cm-wide channel filled with the same sand was installed in the silty clay layer to produce macropore flow (called channel flow in this paper). The test lasted 151 days and the cover system went through two cycles of wetting and drying. Extensive measurements were conducted to investigate water flow, water balance, oxygen concentration and oxidation of the waste rock during the test. This test (referred to as Test 1) is part of experiments performed to investigate the impact of channel flow on the performance of the inclined layered soil cover. This paper is focused on the water flow and water balance aspects of the test. Apart from the test, numerical modeling was conducted using the commercial computer software VADOSE/W to simulate the measured water balance and to analyze the sensitivity of channel flow to water balance components. The objectives of the paper are to (1) present measured water balance in the cover system with channel flow; (2) analyze the effects of the location of the channel and the saturated hydraulic conductivity of the channel material on water balance. The results of the study would help to better understand the effects of preferential flow on cover performance and to enhance cover design to minimize macropore flow.

Materials and methods

Materials

The sand and silty clay used in the study as cover materials were obtained from a location near a suburban area of London, ON, Canada. The waste rock was obtained from Mattabi mine site near Ignace, ON, Canada. The waste rock was crushed, sieved, and washed before being used in the experiments. The particle size distributions of the test materials are presented in Online Resource Graph 1 and the geotechnical properties in Table 1. The detailed description and the elemental compositions of the soils have been described elsewhere by Song and Yanful (2009a). The acid base accounting (ABA) analysis (MEND 1991) indicated that the waste rock was a potential acid producer.

Table 1 Summary of hydraulic and geotechnical properties of soils used in the experiment

	Waste rock	Silty clay	Sand
Saturated hydraulic conductivity (cm/s)	$(3.1 \times 10^{-2})^{a}$	9.5×10^{-9}	2.8×10^{-2}
Plasticity index (%)	–	14.5	–
Optimum water content (%)	–	15.8	–
Dry density (g/cm^3)	2.10	1.81	1.57
Porosity	0.26	0.36	0.41

[a] Value obtained from Hazen's equation based on the particle size distribution

Experimental unit and installation of soils

The cover soils and waste rock were placed in a plastic box measuring 120 cm × 120 cm × 25 cm (width × height × thickness). The box sat on a steel frame and was reinforced with steel angles. A rainfall simulator designed to model field precipitation was placed over the box during rainfall events. Two outlets were installed at the left side of the box and three at the bottom to collect effluents (Fig. 1). Song and Yanful (2009a) have provided a detail description of the experimental unit and the rainfall simulator.

The inclined multilayer test cover consisted of construction sand overlying a compacted silty clay, which, in turn, overlaid crushed acid generating mine waste rock. The thickness of the sand was 30 cm, the compacted silty clay was 50 cm, and the thickness of the waste rock ranged from 11 to 35 cm to provide a 20% slope to support the overlying

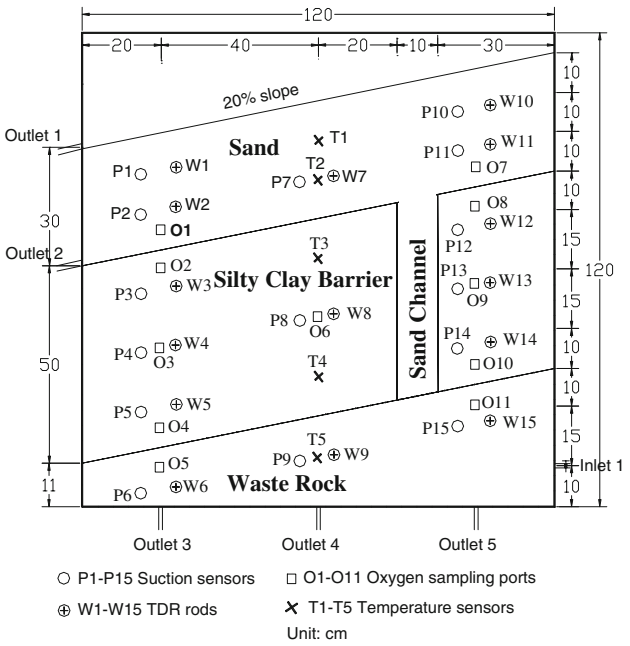

Fig. 1 Section of the soil cover with channel pathway and instruments in the test

cover soils. A 10-cm-wide channel filled with the same construction sand was installed in the silty clay layer to simulate channel or preferential flow in the barrier layer during precipitation events (Test 1). A cross-section of the soil layers and instrumentation is shown in Fig. 1. The channel pathway was located at the upslope section (30 cm from the highest point on the slope). The silty clay was firstly compacted in 5-cm-thick sublayers outside the box, and then transferred into the box. The controlling gravimetric water content of the compacted silty clay was 17.8% (+2% of optimum water content) to achieve a low hydraulic conductivity (Mitchell et al. 1965; Daniel and Benson 1990; Taha and Kabir 2005). The details of the installation of the soils are described elsewhere (Song and Yanful 2009a).

Measurements and data collection

During the test, the temperature and matric suction were recorded hourly through a datalogger. The volumetric water content was measured daily using time-domain reflectometry (TDR) (Topp et al. 1980). Gaseous oxygen in the soils and waste rock were sampled every 3 days and analyzed using an oxygen analyzer for the oxygen concentration. As shown in Fig. 1, there were 5 temperature probes (labeled T1–T5), 15 suction sensors (P1–P15), 15 pairs of water moisture rods (W1–W15), and 11 oxygen sampling ports (labeled O1–O11) employed in the experiment. Moreover, all effluents (runoff, interflow, percolation) and influent (precipitation) were recorded to evaluate the water balance. Samples of the effluents were also analyzed for chemical composition. Air temperature and relative humidity in the laboratory were measured daily during the test. These environmental data are necessary for the modeling of the measured water balance. The test lasted 5 months from 8 February 2008 to 8 July 2008.

Water balance evaluation

As there was negligible runoff, the following equation (Eq. 1) was used to calculate the water balance:

$$V_{\text{preci}} - V_{\text{intf}} - V_{\text{perc}} - V_{\text{evap}} = \pm V_{\text{stor}} \quad (1)$$

where V_{preci} is the total volume of precipitation (m^3), V_{intf} is the total volume of interflow (m^3), V_{perc} is the total percolation (m^3), V_{evap} is the total actual evaporation (m^3), and V_{stor} is the total change in water storage of the test soils (m^3). A positive value of the change in water storage means the total water content increases in the cover system, while a negative value indicates the total water content decreases. Total change in water storage was calculated from the measured volumetric water content of the soils. Due to the heavy weight of the test box and the soils, the actual evaporation from the system was not directly measured

from weighing but was calculated from Eq. 1. In the computer program VADOSE/W, the actual evaporation from the system was calculated directly from the Penman-Wilson method (Wilson 1990) or input potential evaporation, while the percolation was estimated using Eq. 1 when runoff was negligible.

Modeling

Modeling methodology

The computer program VADOSE/W (GEO-SLOPE 2004) couples heat transport and water transfer to simulate flow of water, heat and vapor through both saturated and unsaturated soils. The embedded oxygen transfer (modified Fick's second law) is dependent on the saturation of the soils but does not influence the calculation of the heat and water flow part, so the water flow part can be simulated separately. The basic governing equations for the water flow and heat transport are as follows (Eqs. 2, 3).

$$m\frac{\partial P}{\partial t} = Q + \frac{1}{\rho_w}\frac{\partial}{\partial x}\left(D_v\frac{\partial P_v}{\partial x}\right) + \frac{1}{\rho_w}\frac{\partial}{\partial y}\left(D_v\frac{\partial P_v}{\partial y}\right) + \frac{\partial}{\partial x}\left(K_x\frac{\partial(P/\rho_w g + y)}{\partial x}\right) + \frac{\partial}{\partial y}\left(K_y\frac{\partial(P/\rho_w g + y)}{\partial y}\right) \quad (2)$$

$$\lambda_t\frac{\partial T}{\partial t} = Q_t + L_v\frac{\partial}{\partial x}\left(D_v\frac{\partial P_v}{\partial x}\right) + L_v\frac{\partial}{\partial y}\left(D_v\frac{\partial P_v}{\partial y}\right) + \frac{\partial}{\partial x}\left(k_{tx}\frac{\partial T}{\partial x}\right) + \frac{\partial}{\partial y}\left(k_{ty}\frac{\partial T}{\partial y}\right) + \rho_w c_w V_x\frac{\partial T}{\partial x} + \rho_w c_w V_y\frac{\partial T}{\partial y} \quad (3)$$

where P is water pressure, m is the slope of the soil water characteristic curve, Q is the applied boundary flux, P_v is vapor pressure of the soil moisture, D_v is the vapor diffusion coefficient, K_x and K_y are hydraulic conductivity in the x and y directions, respectively, y is elevation head, ρ_w is density of water, g is acceleration due to gravity and t is time, λ_t is apparent volumetric heat capacity of soil, T is temperature, Q_t is the applied thermal boundary flux, L_v is latent heat of vaporization; k_{tx} and k_{ty} are thermal conductivity values in the x and y directions, respectively, c_w is mass specific heat capacity of water, V_x and V_y are Darcy water velocity in the x and y directions.

Then water (liquid and vapor phases) flow and heat transfer were combined using Eq. 4 (Edlefsen and Anderson 1943).

$$P_v = P_{vs}\left(e^{\frac{-PW_v}{\rho_w RT}}\right) \quad (4)$$

where P_{vs} is saturated vapor pressure of pure free water, W_v is the molecular weight of water (0.018 kg/mol), R is universal gas constant (8.314 J/mol K).

Actual evaporation (E) is calculated using the Penman-Wilson method (Wilson 1990) when net surface radiation data are available (Eq. 5) or directly estimated from user supplied potential evaporation (Eq. 6).

$$E = \frac{\Delta Q_n + \upsilon E_a}{\Delta + A\upsilon} \quad (5)$$

where E is actual evaporation, Δ is slope of the saturation vapor pressure versus temperature curve at the mean temperature of the air, Q_n is net radiant energy available at the surface, υ is the psychometric constant, $E_a = f(u)e_a(B - A)$, $f(u) = 0.35(1 + 0.15\ U)$, U is wind speed, e_a is vapor pressure in the air above the evaporating surface, B is inverse of the relative humidity of the air, A is inverse of relative humidity at the soil surface.

$$E = E_p\left(\frac{h_r - (e_{sa}/e_{ss})h_a}{1 - (e_{sa}/e_{ss})h_a}\right) \quad (6)$$

where E_p is user supplied potential evaporation, h_r is relative humidity at the soil surface, h_a is relative humidity of the air, e_{sa} is saturation vapor pressure in the air above the evaporation surface, e_{ss} is saturation vapor pressure at the soil surface. In VADOSE/W, Eqs. 2–6 are solved simultaneously using finite elements and input data to yield the actual evaporation rate E, the vapor pressure P_v, water pressure P, and temperature T. Key input data include the soil–water characteristic curve (SWCC), the hydraulic conductivity–suction function, thermal data (soil thermal conductivity, mass specific heat capacity), and climate data (temperature, relative humidity, wind speed, precipitation). Other details on VADOSE/W are given in Krahn (2004).

The measured water balance components were first employed to calibrate and validate the input parameters in the computer program VADOSE/W. Then further analysis of channel flow was conducted using the calibrated program. Two aspects were investigated in the present study: the effects of the location of the channel on the components of water balance and the effects of material property (i.e., saturated hydraulic conductivity) of the sand filling the channel pathway on water balance components. The purpose was to obtain a picture of how channel flow occurring in the moisture-retaining layer impacts the long-term performance of the soil cover. Table 2 presents the modeling cases and their purposes. Case 1, the experimental case, was to calibrate the model. The effect of the location of the channel flow pathway on the water balance was modeled through Cases 2–5. The location of the channel pathway in the current study is expressed by the normalized distance (x), which is defined as the ratio of the horizontal distance from the mid-point of the channel pathway to the highest point on the slope to the total horizontal length of the soil cover. In all the modeling cases, the width of the channel pathway was 10 cm, the same as that built in the

Table 2 Modeling cases in the present study

Modeling case	Type of case	Purpose	Properties of the channel pathway		
			Specific position-horizontal distance from the highest point on the slope (cm)	Normalized distance[a] (x, m/m)	Saturated hydraulic conductivity (m/day)
Case 1	Experimental test (Test 1)	To calibrate model	Upslope, 30–40	0.29	24.2
Case 2	Hypothetical case	To evaluate the effect of the location of the channel pathway on water balance	Up-upslope, 0–10	0.04	24.2
Case 3	Hypothetical case		Midslope, 60–70	0.54	24.2
Case 4	Hypothetical case		Downslope, 80–90	0.71	24.2
Case 5	Hypothetical case		Down-downslope, 110–120	0.96	24.2
Case 6	Hypothetical case	To evaluate the effect of hydraulic conductivity of material filling the channel pathway on water balance	Upslope, 30–40	0.29	242
Case 7	Hypothetical case		Upslope, 30–40	0.29	121
Case 8	Hypothetical case		Upslope, 30–40	0.29	48.4
Case 9	Hypothetical case		Upslope, 30–40	0.29	12.1
Case 10	Hypothetical case		Upslope, 30–40	0.29	4.84
Case 11	Hypothetical case		Upslope, 30–40	0.29	2.42

[a] Normalized distance (x) is the ratio of the horizontal distance from the mid-point of the channel pathway to the highest point on the slope to the total horizontal length of the soil cover, e.g. for Case 1, the normalized distance = 0.35 m/1.20 m = 0.29

experiment. The material filling the channel pathway and its hydraulic properties (specifically, SWCC and unsaturated hydraulic conductivity) were also the same as in the experiment.

In addition, six other cases (Cases 6–11) were modeled to analyze the influence of the saturated hydraulic conductivity of the channel material on the water balance. In this modeling, the location of the channel and its width were kept the same as that built in the experiment. As mentioned, the SWCC of the channel material was also kept unchanged. Only the saturated hydraulic conductivity of the material was varied.

Figure 2 shows the finite element mesh used to model the water balance in the experiment. A finer mesh (1 cm high) was chosen at the surface 20 cm in the sand layer to improve computation accuracy and convergence. The drying and wetting processes in the experiment were modeled separately for the sand layer. It was somewhat a pseudo-hysteretic analysis because only the unsaturated hydraulic conductivity functions were varied during the drying and wetting processes and the SWCC of the sand was kept the same to simplify the modeling. Only the sand layer was considered during separate drying and wetting stages in the modeling because: (1) the measured water content and matric suction in the sand layer showed significant difference during the precipitation and evaporation stages; (2) the water content and the suction in the silty clay layer and the waste rock were relatively stable during the precipitation and evaporation stages. Apart from the consideration of the different drying and wetting processes in the sand layer, the surface sublayer (0–10 cm) of the sand was assigned different unsaturated hydraulic conductivity values during rainfall events to consider the initial infiltration process (Krahn 2004). The thickness of the top sublayer of the sand was taken as 10 cm based on a visual examination of the sand layer in the experimental unit, which revealed a relatively dry sublayer 4–9 cm at the surface along the slope before rainfall events. The modeling steps and the corresponding unsaturated hydraulic conductivity functions of the sand layer for the experimental case are presented in Table 3. Other modeled hypothetical cases also followed the same modeling steps as listed in Table 3. However, for Cases 6–11, the saturated hydraulic conductivity of the material filling the channel pathway was changed (but the shape of the unsaturated hydraulic conductivity curve was kept the same as that of the sand layer at the depth of 10–30 cm).

Input data

Data needed to run VADOSE/W include soil properties (SWCC, unsaturated hydraulic conductivity, thermal data) and environmental and climatic conditions (temperature, relative humidity, wind speed, potential evaporation, and precipitation). In addition, the oxygen decay coefficient of the waste rock must also be known in order to calculate the gas flux.

Soil water characteristic curve The soil–water characteristic curve (SWCC) of a soil is an important parameter that governs water movement in the unsaturated soil. The SWCC tests of the waste rock and sand were conducted using a tensiometer with a measurement range of 0–100 kPa. The SWCC of the silty clay was measured using a pressure plate (Fredlund and Rahardjo 1993) that could withstand a maximum air pressure of 15 bars (approximately

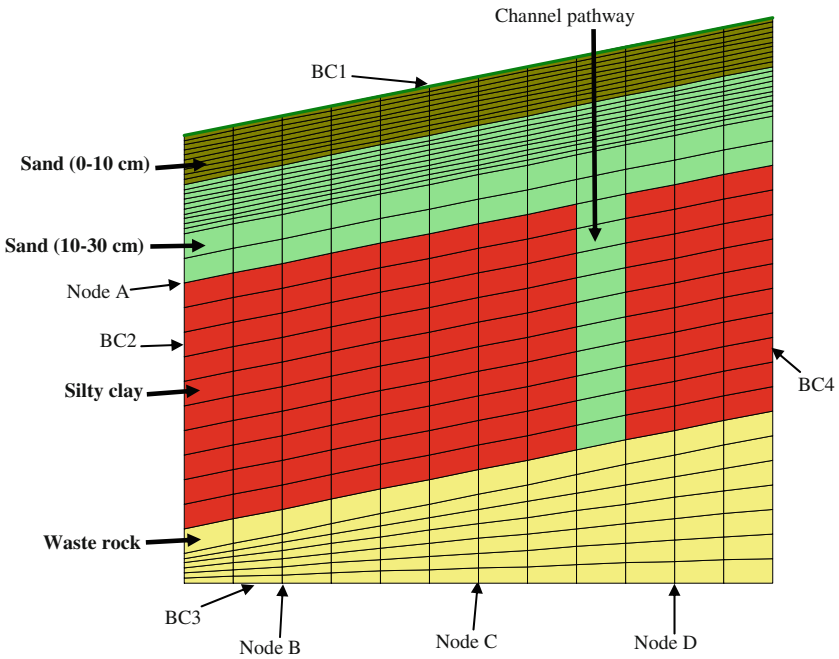

Fig. 2 Mesh and boundary conditions used in the computer modeling (*BC* boundary condition)

Table 3 Modeling steps applied in the present study for Case 1 (experimental case)

Modeling step	Modeling period	Climatic event	Used unsaturated hydraulic conductivity of the sand layer as shown in Fig. 4
Step 1	18 days from 8 to 25 February 2008	Drying stage	The whole sand layer used the hydraulic conductivity curve labeled "sand-drying"
Step 2	6 days from 26 February to 2 March 2008	Raining stage (first rainfall event)	The surface sand 10 cm used the hydraulic conductivity curve labeled "sand (0–10 cm)-wetting", and other sand (including sand in the channel path) used the curve labeled "sand (10–30 cm)-wetting"
Step 3	61 days from 3 March to 2 May 2008	Drying stage	The whole sand layer used the hydraulic conductivity curve labeled "sand-drying"
Step 4	7 days from 3 to 9 May 2008	Raining stage (second rainfall event)	The surface sand 10 cm used the hydraulic conductivity curve labeled "sand (0–10 cm)-wetting", and other sand (including the sand in channel path) used the curve labeled "sand (10–30 cm)-wetting"
Step 5	60 days from 10 May to 8 July 8 2008	Drying stage	The whole sand layer used the hydraulic conductivity curve labeled "sand-drying"

1,500 kPa). The measured data were fitted with the equation by Fredlund and Xing (1994). Figure 3 shows the SWCCs of the test soils used in the modeling. The fitted parameters are listed in Table 4.

Unsaturated hydraulic conductivity function The unsaturated hydraulic conductivity functions of the soils used in the modeling are shown in Fig. 4. These curves were obtained by fitting the saturated hydraulic conductivity of the soils and the corresponding SWCCs with the function embedded in VADOSE/W. The methods used to obtain the saturated hydraulic conductivity of the soils have been described by Song and Yanful (2009a). The van Genuchten (1980) model was used to generate the unsaturated hydraulic conductivity functions for all soils except the sand in the wetting stage which was fitted with the method proposed by Fredlund et al. (1994). The saturated hydraulic conductivity of the waste rock was decreased from 3.1×10^{-2} to 1.16×10^{-3} cm/s to consider the effect of the underlying geotextile because it was found that fine particles collecting on the geotextile blocked the water flow significantly and delayed percolation during the test. The unsaturated hydraulic conductivity functions for the sand were slightly modified during calibration of the model. During precipitation events (wetting stage), only 2–3 orders of magnitude increase in the unsaturated hydraulic conductivity of the sand [labeled "Sand (0–10 cm)-wetting" in Fig. 4] was assigned to the surface sublayer

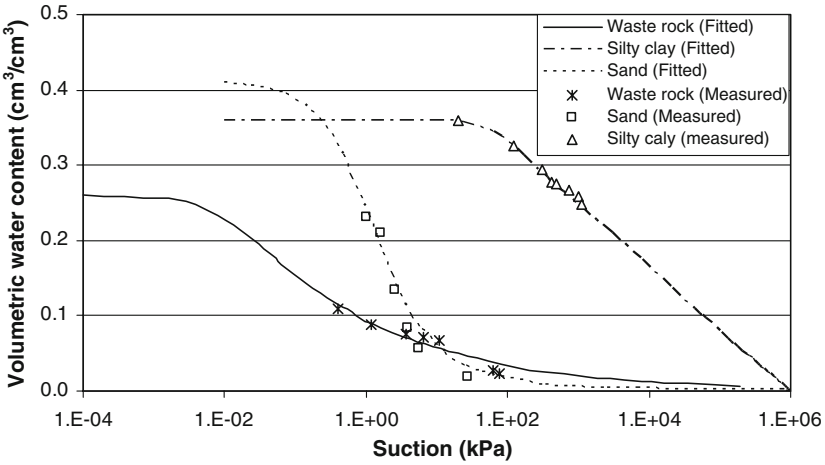

Fig. 3 Soil water characteristic curves measured from the experiments and fitted with equation by Fredlund and Xing (1994)

Table 4 Input thermal data and curve fitted parameters used for the cover soils and waste rock in the modeling

Soil	Mass specific heat capacity (kJ/kg °C)	Soil mineral thermal conductivity (kJ/day m °C)	Parameters[a]		
			a	*n*	*m*
Sand	0.88	380	0.99566	1.094	1.9288
Silty clay	0.8	400	88.894	1.7143	0.23098
Waste rock	0.7	388	0.03401	0.72593	1.0855

[a] Parameters used in the equation by Fredlund and Xing (1994)

(Krahn 2004). The sand filling the channel pathway had the same unsaturated hydraulic conductivity as the sand layer overlying the barrier, that is, at the depth of 10–30 cm. During analysis of the effects of the saturated hydraulic conductivity of channel sand on the water balance, the channel sand had the same unsaturated hydraulic conductivity–suction function (same shape) as the sand layer at the depth of 10–30 cm, but different saturated hydraulic conductivity.

Thermal data The mass specific heat capacity and thermal conductivity of the soil are two input parameters in VADOSE/W that define the heat transfer in the soil. The water content and thermal behavior of the soil can influence each other because unsaturated soil consists of air, water and solid particles, and air and water have different thermal behavior. Table 4 lists the thermal data for the soils used in the modeling.

Climate data The climate data needed in VADOSE/W include daily minimum and maximum temperature, daily minimum and maximum relative humidity, daily wind speed, daily energy source (net radiation or potential evaporation) and precipitation and its duration. Generally, the change in temperature during the experiment was not large (about 6°C), and the daily change in laboratory temperature was around 2–3°C (Online Resource Graph 2). Therefore, the minimum temperature used in the model was the measured temperature minus 1°C and the maximum temperature was the measured temperature plus 1°C. The average humidity ranged from 12 to 60%. The difference between the maximum and the minimum humidity was mostly less than 10%. A table fan positioned above the experimental unit provided wind for the soil cover. The potential evaporation measured downslope and upslope of the sand surface indicated that the wind speed was not uniform along the slope. The wind speed upslope was higher than that downslope. The estimated average wind speed was 2.6 m/s when the fan was on. The wind speed was zero when the fan was off. During the modeling, the measured potential evaporation was input for the calculation of actual evaporation and its distribution was considered constant each day. The measured average potential evaporation was 1.8 mm/day when the fan was switched off and 3.8 mm/day when the fan was turned on. During the test period, the soil cover had two rainfall stages. The first rainfall event, applied over 6 days from 26 February to 2 March 2008, had a total precipitation of 164 mm and an average intensity of 27.3 mm/day. The second rainfall event lasted 7 days (from 3 to 9 May 2008) and had a total precipitation of 148.1 mm and an average intensity of 21.2 mm/day (Online Resource Graph 3).

Boundary and initial conditions

The boundary conditions applied in the modeling are indicated in Fig. 2 and explained in Table 5. The measured indoor climate data were employed as the upper boundary condition (BC1). At the bottom of the waste rock, Nodes B, C and D (at the locations of Outlets 3, 4 and 5 in Fig. 1) were specified as seepage points during modeling, and the

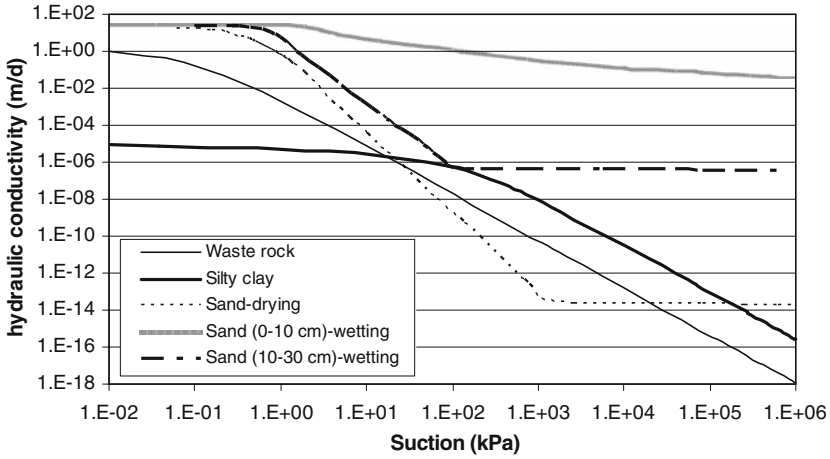

Fig. 4 Unsaturated hydraulic conductivity used in the modeling

Table 5 Boundary conditions used in modeling

Symbols used in Fig. 2	Location	Explanation
BC1	Surface of the soil cover (upper boundary)	Climate data without vegetation data
BC2 (except for Node A)	Left side of the soil cover (downdip boundary)	Zero water flux, zero thermal flux, and zero gas flux
BC3 (except for Nodes B, C, and D)	Bottom of the soil cover (bottom boundary)	Zero water flux, zero thermal flux, and zero gas flux
BC4	Right side of the soil cover (updip boundary)	Zero water flux, zero thermal flux, and zero gas flux
Node A	Located at the Outlet 2 (Fig. 1)	Seepage point for water flow during rainfall events, zero water flux during drying period. Zero thermal flux and gas flux all time in the modeling
Node B	Located at the Outlet 3 (Fig. 1)	Seepage point for water flow, zero thermal flux and gas flux
Node C	Located at the Outlet 4 (Fig. 1)	Seepage point for water flow, zero thermal flux and gas flux
Node D	Located at the Outlet 5 (Fig. 1)	Seepage point for water flow, zero thermal flux and gas flux

other nodes at the base (BC3) were set as no-flux boundary. The right side (BC4) was specified as no-flux condition, and the left side (BC2) was also specified as no-flux boundary except for Node A (at the location of Outlet 2 in Fig. 1), which was specified as seepage point during precipitation and no-flux point during drying period. The boundary conditions for heat transport and gas diffusion were very simple. Except for the upper boundary (climate boundary), the other three sides were set to a no-flux boundary for heat transport and gas diffusion.

The initial parameters needed for the nodes were pressure, temperature, and gaseous oxygen concentration. For pressure, −0.8, −0.3, and −0.1 m were specified for the nodes in the sand layer, silty clay layer, and waste rock, respectively. These values were similar to the measured soil water potential values downslope in the sand layer, silty clay layer, and waste rock at the beginning of the test. The temperature was kept constant at 22°C, and the initial gaseous oxygen concentration was 180 g/m^3.

Results

Soil temperature, matric suction, and volumetric water content

In general soil temperature during the experiments changed with the air temperature in the laboratory; temperatures in the soils were very close to each other in the range of 20–24°C. The temperature fluctuated more in the sand layer than in the silty clay layer and the waste rock because the sand layer, being the upper most layer, was in direct contact with the atmosphere. The measured laboratory temperature was about 1–1.5°C higher than the measured temperature in the soils (Online Resource Graph 4).

At the same depth in the sand layer, the measured matric suction increased upslope during the drying period (Fig. 5). For example, the suction upslope was 34.5 kPa at the end of the first wetting–drying cycle (2 May 2008), while suctions midslope and downslope were 24 and 18.5 kPa,

respectively. Similarly, the measured matric suctions at the end of the test (8 July 2008) were 30, 20, and 14 kPa upslope, midslope, and downslope, respectively. Although the sensor located midslope was equidistant from the ones upslope and downslope, the measured suction differences between them were not the same. The difference between the suction upslope and the one midslope was larger than that between the suction midslope and the suction downslope. For instance, the suction difference between P11 (upslope) and P7 (midslope) was 10 kPa at the end of the first wetting–drying cycle (2 May 2008), while the suction difference between P7 (midslope) and P2 (down slope) was about 5 kPa on the same day. This phenomenon may be attributed to the effect of the channel pathway and channel flow existing between the upslope and the midslope. Due to water moving down through the channel pathway during rainfall events, less water accumulated upslope, resulting in larger suction during the subsequent dry period. Even during rainfall events, the suction upslope was a bit larger than those midslope and downslope due to the effect of the channel flow upslope. Apart from the effects of channel flow, suction was also influenced by slope because of water movement down the slope. For example, the suction midslope was larger than the one downslope as mentioned above.

The matric suction in the silty clay and sand layers had similar trends (Online Resource Graph 5). In general, rainfall events affected the suction in the silty clay layer because suction decreased during precipitation. Evaporation had less effect on the silty clay layer than on the sand layer due to the lower hydraulic conductivity of the sand layer when suction was high. Measured matric suction values in the middle of the silty clay layer ranged from 0 to 10 kPa. Thus, it may be inferred that the overlying sand layer prevented water loss from the barrier layer (silty clay) during evaporation. Yanful et al. (2003) made similar observations from laboratory experiments. The relatively lower suction measured in the silty clay layer implied that the silty clay layer could maintain high water content at increasing suctions in the overlying sand.

Measured matric suction in the waste rock (Online Resource Graph 6) decreased with time and was not affected by rainfall events, unlike the trends observed in the sand and silty clay. Suction values recorded in the waste rock (depth of 90 cm) were between −1 and 1 kPa. The negative suction values implied that the waste rock was nearly saturated. This was in agreement with the volumetric water content (0.1–0.3 cm^3/cm^3) measured on waste rock samples taken after the test.

The observed volumetric water content of the sand layer at the depth of 20 cm agreed well with measured suction at the same depth (Fig. 6). The volumetric water content decreased along the slope from downslope to upslope. Water was lost more quickly upslope (W11) than midslope and downslope (W7 and W2) following rainfall. The measured maximum volumetric water content in the sand layer at the depth of 20 cm below the sand surface was approximately 0.13 downslope (W2) with a degree of saturation of 32% during the rainfall events, whereas the maximum volumetric water content upslope (W11) was approximately 0.09 with a degree of saturation of 22%. These results indicate that the upslope channel flow pathway likely transported more gaseous oxygen into the underlying waste rock.

As predicted from the measured matric suction, the volumetric water content in the silty clay layer at the depth of 55 cm was close to the porosity and ranged from 0.33 to 0.38 (Fig. 7). The water content downslope was higher than those measured midslope and upslope. Rainfall events did not show much effect on the volumetric water content of the silty clay layer. Because the whole silty clay layer was compacted in ten sublayers, the measured initial water content showed some scatter. After 80 days, the water content of the silty clay layer became relatively uniform

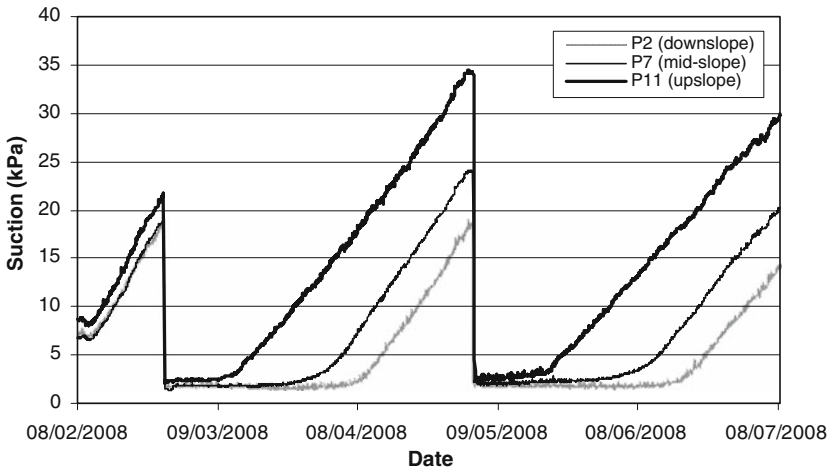

Fig. 5 Measured matric suction in the sand layer at the depth of 20 cm

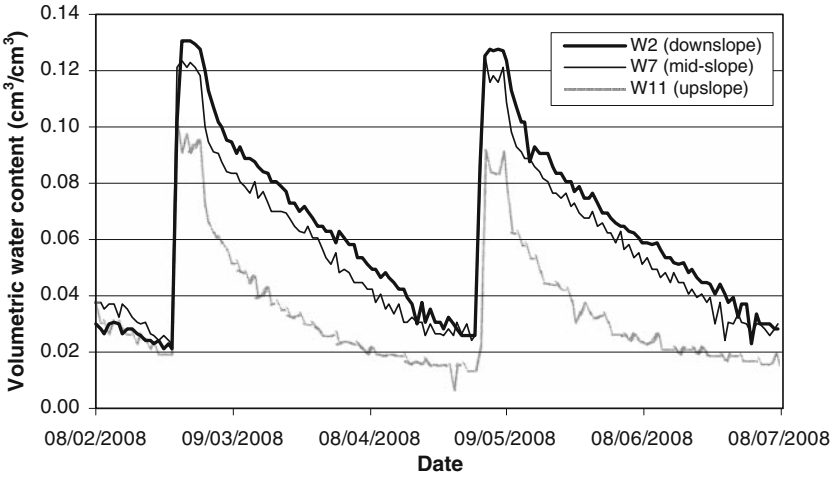

Fig. 6 Measured volumetric water content in the sand layer at the depth of 20 cm

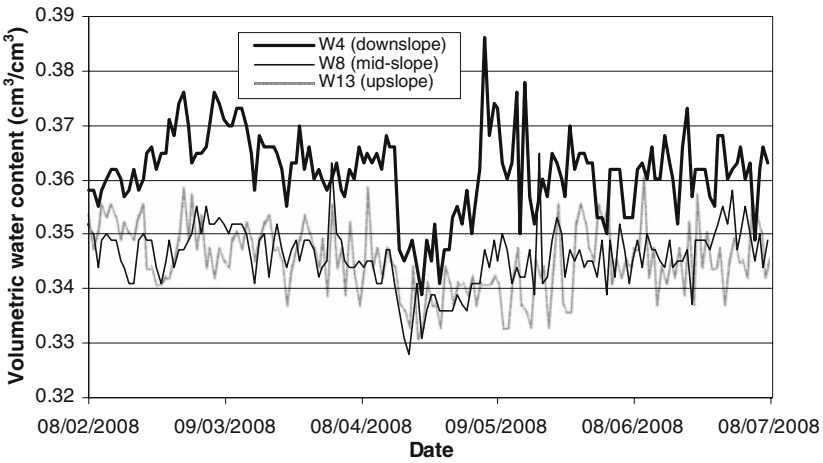

Fig. 7 Measured volumetric water content in the silty clay layer at the depth of 55 cm

due to the re-distribution of the pore water. The average volumetric water content at the depth of 55 cm in the silty clay layer was about 0.35 at the end of the test, which corresponded to a degree of saturation of 97%. This high saturation would considerately reduce gaseous oxygen ingress into the underlying waste rock.

The measured volumetric water content downslope (W6) in the waste rock ranged from 0.03 to 0.06; it was 0.05 and 0.08 midslope (W9) and 0.02–0.035 upslope (W15) (Online Resource Graph 7). TDR measured volumetric water contents of the waste rock likely did not reflect actual values because they were significantly different from water contents (0.1–0.19) obtained from oven drying at the end of the test. Previous study by Song and Yanful (2009b) using column tests with similar precipitation events gave volumetric water content of similar order (0.16, on average). Visual inspection after the test indicated that the waste rock close to the bottom of the box was nearly saturated. Fortunately, the volumetric water content of the waste rock had only a small influence on the calculation of the water storage change in the soil cover system because the change in the waste rock water content was insignificant and the volume of waste rock was smaller than that of the sand or silty clay.

Comparison of modeled and measured water balance components

The modeled and measured water balance components including precipitation, interflow, percolation, actual evaporation, and change in soil water storage for the experimental case (Case 1) are shown in Fig. 8 and in Table 6. Figure 8 indicates that there was almost no discrepancy between the measured precipitation and the precipitation used by the model due to indoor temperature being higher than 0°C during the test period.

The measured total interflow was 33.08 L, while the modeled interflow was 33.07 L; that is, there was only 0.01 L difference in the total interflow. For the percolation, the measured value (40.24 L) was close to the modeled value (38.48 L). The modeled change in soil water storage and actual evaporation also matched the measured values

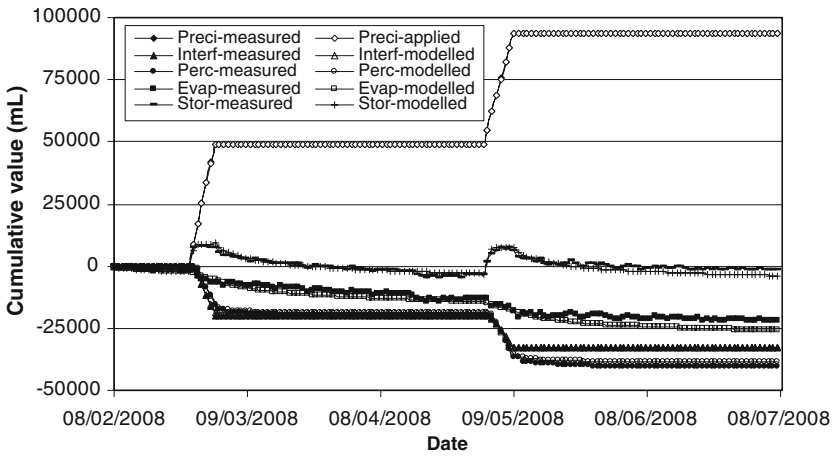

Fig. 8 Comparison of measured and modeled water balance components for the experimental case (Case 1). *Preci* precipitation, *interf* interflow, *perc* percolation, *evap* actual evaporation, *stor* change in soil water storage

Table 6 Measured and modeled water balance components for the experimental case (Case 1)

Components	Measured values (L) and percentage			Modeled values (L) and percentage		
	First rainfall event	Second rainfall event	Total	First rainfall event	Second rainfall event	Total
Precipitation	49.197 (52.5)[a]	44.437 (47.5)	93.634 (100)	49.098 (52.5)	44.497 (47.5)	93.595 (100)
Interflow	20.029 (21.4)	13.051 (13.9)	33.080 (35.3)	18.888 (20.2)	14.182 (15.1)	33.070 (35.3)
Percolation	19.781 (21.1)	20.456 (21.8)	40.237 (43.0)	19.011 (20.3)	19.465 (20.8)	38.476 (41.1)
Change in soil water storage	+7.966[b] (+8.5)	+7.558[b] (+8.1)	−1.741[c] (−1.9)	+9.122[b] (+9.7)	+7.185[b] (+7.7)	−3.833[c] (−4.1)
Actual evaporation			22.058 (23.6)			25.901 (27.7)

[a] The values in the bracket are the percentages over the total precipitation

[b] The maximum values achieved during the rainfall events; the positive value meant the water storage in the cover system increased

[c] The final change in soil water storage in the cover system; the negative value meant that the water storage in the cover system decreased

very well. For example, the modeled cumulative change in soil water storage and actual evaporation at the end of test were −3.83 and 25.90 L, respectively, while the measured cumulative change in soil water storage and actual evaporation were −1.74 and 22.06 L, respectively. As shown in Table 6, the largest difference between modeled and measured water balance components occurred in the actual evaporation with an error of 4.1% (23.6% for measured and 27.7% for modeled actual evaporation) over the total precipitation, which indicated that the modeled water balance components were, in general, consistent with the measured results.

The measured interflow during the second rainfall event (2–9 May 2008) was 13.05 L, which was less than the measured interflow in the first rainfall event (26 February to 2 March 2008) with a value of 20.03 L. This difference implied that lower precipitation intensity produced smaller interflow. However, the measured percolations from the first rainfall event and the second rainfall event were 19.78 and 20.46 L, respectively, which were very close to each other. So, the effects of precipitation intensity on the interflow and percolation were different. Another reason for the difference in behavior between interflow and percolation during the first and second rainfall events may be the presence of the geotextile underneath waste rock in the box. The geotextile could be plugged by fine particles from the waste rock and might not have transferred effluent evenly. The modeled interflow and percolation during the first and second rainfall events had similar results as the measured values. In short, the comparison of modeled and measured water balance components indicated that the model could reasonably predict the measured water balance under the prescribed parameters and designed modeling steps for the experimental case (Case 1).

Results of sensitivity analysis

Figure 9 shows the modeled changes in soil water storage at different locations in the inclined soil covers with the channel flow pathways. The rainfall events increased the total water content in the cover system. Larger precipitation and intensity produced the larger positive change in soil water storage during rainfall. For instance, the maximum changes in soil water storage after the first and the second rainfall events for Case 3 were 8.2 and 5.2%, respectively. With the change of the channel pathway from

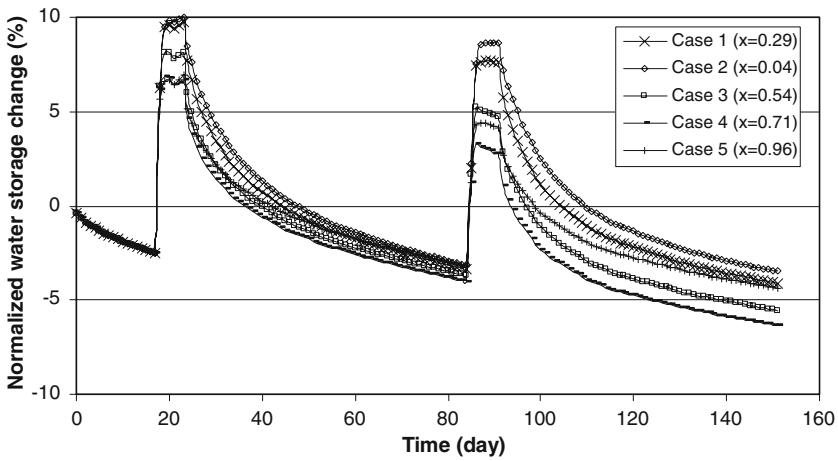

Fig. 9 Modeled changes in soil water storage for the inclined soil covers with the channel flow pathway at the various locations in the barrier layer. Case 1 is the experimental case, Cases 2–5 are the hypothetical cases, and the normalized distance (x) is the ratio of the horizontal distance from the mid-point of the channel pathway to the highest point on the slope to the total horizontal length of the soil cover

the upslope to the downslope (i.e., increasing the normalized distance of the channel pathway, x), the maximum change in soil water storage decreased. For example, the maximum change in soil water storage was approximately 9.7% for Case 1 ($x = 0.29$) during the first rainfall event, while the maximum change in soil water storage was around 6.8% for Case 4 ($x = 0.71$) during the same period. Similar results can be found in the second rainfall event.

The change in soil water storage decreased quickly after rainfall but further decreased slowly with the prolonged dry period. The normalized changes in soil water storage were very close to each other (around −4%) at the end of the first wet–dry cycle (day 84 in Fig. 9) but were a bit scattered at the end of the second wet–dry cycle (e.g., the changes in soil water storage in Cases 1, 3, and 4 were −4.1, −5.5, and −6.3%, respectively on day 151) for the different locations of the channel pathway. The difference in the water storage change for the modeled cases during the first and the second wet–dry cycles may be attributed to the varying indoor climate. During the first wet–dry cycle, the average relative humidity in the laboratory was 10–30%, but it ranged from 20 to 60% in the second wet–dry cycle, as shown in Online Resource Graph 2. The higher relative humidity caused less evaporation, thereby decreasing the change in water content.

The relationship of normalized interflow, percolation, and actual evaporation to the location of the channel flow pathway is presented in Table 7 (also Online Resource Graph 8). With the location of the channel pathway changing from upslope to downslope (i.e., increase in the normalized distance of the channel pathway, x), the calculated percolation increased from 20.8 to 80.1%, and interflow decreased from 53.1 to 0%. However, the estimated interflow accounted for a very small part (<2.5%) after the normalized distance of the channel pathway was larger than 0.71 (Table 7). Similarly, percolation reached the maximum value of 80.1% when $x = 0.71$ (Case 4) and did not increase with an increase in the normalized distance of the channel pathway. The actual evaporation from the soil covers declined from 30.1 to 23.9% with the increase in the normalized distance of the channel pathway from $x = 0.04$ (Case 2) to $x = 0.71$ (Case 4). When the distance of the channel increased from $x = 0.71$ to 0.96 (Case 5), the actual evaporation only increased from 23.9 to 24.2%. As shown in Table 7, the sum of percolation and interflow increased from 73.9 to 82.6% with increasing normalized distance of the channel pathway from $x = 0.04$ to 0.71. When the distance of the channel increased from $x = 0.71$ to 0.96, the sum of percolation and interflow decreased from 82.6 to 80.1%. Similarly, the sum of percolation,

Table 7 Modeled percolation, interflow, and actual evaporation for the soil cover with the channel pathway at the various locations (Cases 1–5)

Normalized distance[a] (x, m/m)	Modeling cases	Normalized value (%)			Sum of percolation, interflow (%)	Sum of percolation, interflow, actual evaporation (%)
		Percolation	Interflow	Actual evaporation		
0.04	Case 2	20.8	53.1	30.1	73.9	104.0
0.29	Case 1	41.1	35.3	27.7	76.4	104.1
0.54	Case 3	65.7	14.8	25.1	80.5	105.6
0.71	Case 4	80.1	2.5	23.9	82.6	106.5
0.96	Case 5	80.1	0	24.2	80.1	104.3

[a] Normalized distance (x) is the ratio of the horizontal distance from the mid-point of the channel pathway to the highest point on the slope to the total horizontal length of the soil cover

interflow, and actual evaporation also increased with an increase in the normalized distance of the channel pathway from the highest point on the slope (x) and reached a maximum value of 106.5% at $x = 0.71$ (Case 4), and then decreased with further increase in the normalized distance. Generally, the sum of percolation, interflow, and actual evaporation was relatively constant (in the range of 104–106.5%) as the channel pathway moved from upslope to downslope.

When the location of the channel flow pathway was kept constant at the normalized distance of 0.29 (the same as in the experiment), changes in soil water storage with time for the varying saturated hydraulic conductivity (K_s) values of the sand filling the channel (Cases 1 and 6–11) are shown in Fig. 10. With a decrease in the saturated hydraulic conductivity of the material filling the channel pathway, the change in soil water storage increased during the rainfall events. For example, the change in soil water storage was about 8.8% during the first rainfall event (days 18–23) for Case 6 ($K_s = 242$ m/day) and 10.9% for Case 11 ($K_s = 2.42$ m/day) over the same period. For all the modeled cases, the change in soil water storage was larger during the first rainfall event (days 18–23) than during the second rainfall event (days 85–92). Again, this can be attributed to the effect of precipitation intensity because the average intensity during the first rainfall events (27.3 mm/day) was larger than that in the second rainfall events (21.2 mm/day). The changes in soil water storage for all modeled hydraulic conductivities ranged from −2.8 to −3.6% at the end of the first wet–dry cycle (day 84) and from −2.8 to −4.9% at the end of the second wet–dry cycle (day 151).

Table 8 presents the modeled calculated interflow, percolation, and actual evaporation for the cover when the material filling the channel pathway had different saturated hydraulic conductivity (K_s) values (Cases 1 and 6–11). Normalized interflow, percolation, and actual evaporation changed significantly more with a change in the saturated hydraulic conductivity (K_s) of the channel material when K_s was less than 48.4 m/day (twice the hydraulic conductivity of the overlying sand layer) than the cases when K_s was larger than 48.4 m/day (Online Resource Graph 9). In general, actual evaporation did not change as much as interflow and percolation in all modeled cases. Table 8 shows that the sum of modeled percolation and interflow and the sum of percolation, interflow, and actual

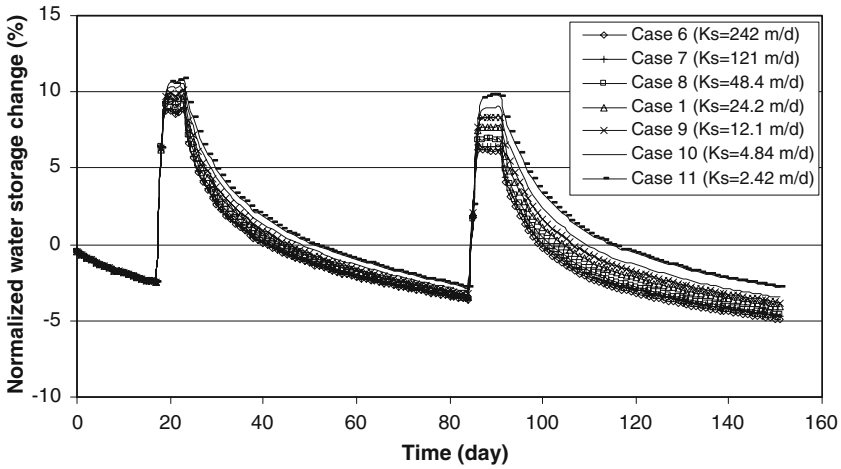

Fig. 10 Modeled changes in soil water storage for the inclined layered soil cover with the material filling the channel pathway having varying saturated hydraulic conductivities. Case 1 is the experimental case, Cases 6–11 are the hypothetical cases

Table 8 Modeled results of percolation, interflow, and actual evaporation for the soil cover with the material filling the channel pathway having varying saturated hydraulic conductivity values (Cases 1 and 6–11)

Saturated hydraulic conductivity (m/day)	Modeling cases	Normalized value (%)			Sum of percolation, interflow (%)	Sum of percolation, interflow, actual evaporation (%)
		Percolation	Interflow	Actual evaporation		
242	Case 6	51.9	26.8	26.2	78.7	104.9
121	Case 7	50.0	28.3	26.4	78.3	104.7
48.4	Case 8	46.1	31.3	27.1	77.4	104.5
24.2	Case 1	41.1	35.3	27.7	76.4	104.1
12.1	Case 9	34.8	40.4	28.6	75.2	103.8
4.84	Case 10	24.9	48.8	29.7	73.7	103.4
2.42	Case 11	17.4	54.7	30.7	72.1	102.8

evaporation decreased with a decrease in the saturated hydraulic conductivity of the material filling the channel. However, the decrease in the sum of percolation, interflow, and actual evaporation was small and ranged from 104.9% with $K_s = 242$ m/day (Case 6) to 102.8% with $K_s = 2.42$ m/day (Case 11), as shown in Table 8.

Discussion

After the test, several samples were taken from each soil layer to measure water content using the oven drying method. The results showed that TDR measured volumetric water contents of the sand and silty clay agreed well with those obtained from oven drying. However, the TDR measured volumetric water contents of the waste rock showed significant deviation from those obtained from the oven drying method. For example, the TDR measured volumetric water contents ranged from 0.02 to 0.08 (Online Resource Graph 7), while values from oven drying were from 0.1 to 0.19. The discrepancy between the TDR water contents and those from oven drying may be attributed to the effect of the ionic strength of the waste rock pore water on the TDR readings (Nadler et al. 1999; Nichol et al. 2003). These authors have shown that high ionic strength of soil pore water can reduce the quality of TDR waveforms. A further proof that ionic strength played a role was the fact that the TDR measured volumetric water content values and those from oven drying were similar in Test 2 (cover without channel), where the waste rock oxidized less (Song and Yanful 2009a). As mentioned before, the calculated total change in soil water storage in the cover system fluctuated only slightly for the different values of the volumetric water content in the waste rock. However, it would still be necessary to improve the method of measuring the water content of waste rock in future research.

During the test, an electric table fan was placed over the experimental box to create wind to accelerate evaporation from the soil cover. It was found that the equivalent wind speed back-calculated from the measured potential evaporation was not uniform along the surface of the cover slope. The wind speed upslope was higher than the one downslope. This was also confirmed by the fact that the measured matric suction in the sand layer upslope was larger than that downslope at the same depth (say 10 cm), and the upslope section had thicker visible drying front than the downslope. For example, the visible drying front was approximately 4 cm downslope and 9 cm upslope at the end of the test. The difference in the upslope and downslope wind speed made it difficult to set the atmospheric boundary condition at the surface of the soil cover during the modeling. The sensitivity analysis indicated that the different settings of the surface boundary condition produced larger effects on the matric suction simulation in the sand layer (particularly in the top 15 cm) than on the water balance components such as the change in soil water storage.

To calibrate the computer model to measured water balance in the test, the unsaturated hydraulic conductivity functions of the sand layer estimated from the van Genuchten (1980) and Fredlund et al. (1994) methods were decreased slightly in the low suction range (less than 100 kPa) (Online Resource Graph 10). The practice of making slight modifications in input parameters during calibration of saturated–unsaturated flow models has been used by other investigators. For example, Scanlon et al. (2002) used modified laboratory-measured water retention and saturated hydraulic conductivity data generated by UNSAT-H calibration to predict water balance components. Adu-Wusu et al. (2007) also modified laboratory-measured soil water characteristic curves during calibration of model VADOSE/W for water balance prediction in two soil covers. The variability of soil properties implied that the ability of the computer model and accuracy of input parameters are of equal importance in obtaining good outputs from the model (Adu-Wusu et al. 2007).

Although the sand layer went through the apparent wetting and drying periods in the test, its actual hysteresis on SWCC was not considered and only one SWCC (measured in the laboratory using tensiometer with wetting process) was used during modeling because (1) studies (Yang et al. 2004; Pham et al. 2005) have indicated that suction difference between the wetting and drying boundary SWCCs at the same water content in fine sand was only 0.1–0.2 log-cycles; (2) using one SWCC can simplify the modeling. Because VADOSE/W (GEO-SLOPE 2004) does not consider hysteresis, it was difficult to model the actual hysteretic process in detail. In the modeling, the wetting periods were roughly determined just from the rainfall events, but this determination did not represent the actual conditions for the whole sand layer. For example, the drying process may still exist in the sand layer (or part of the sand layer) on the rainy day because the actual precipitation only occurs in 1 h of the rainy day. Moreover, the history of the wetting–drying cycles also affected the hydraulic property and consequently the modeled results. For example, the discrepancies between the measured change in soil water storage, actual evaporation and the corresponding modeled values in the second wet–dry cycle (3 May to 8 July 2008) are relatively larger than those in the first wet–dry cycle (26 February to 2 May 2008) as shown in Fig. 8. This phenomenon implied that the hydraulic properties (SWCC and unsaturated hydraulic conductivity) of the sand may need to be modified slightly for the second wet–dry cycle to get better fit between measured and modeled results.

In the modeled cases with the different saturated hydraulic conductivity values (Cases 6–11), the soil water characteristic of the channel material was unchanged and kept the same as that of the sand used in the experiment. This may not be true in actual field situations because different saturated hydraulic conductivities imply that the materials have varying pore sizes and connectivities which could result in different soil water retention functions. However, the modeled cases still provided insight into the effect of hydraulic conductivity of the filling material in the channel pathway on water balance components during preferential flow in the barrier layer.

In the experiment, the diversion capacity of the barrier layer (silty clay) was likely negligible because of the low saturated hydraulic conductivity (8.2×10^{-6} m/day) of the silty clay layer and the short length of the soil cover. The channel flow could have a different effect on the water balance components if a large diversion capacity can be built up at the bottom of a capillary barrier and the scale of the soil cover is large. Except for the location of the preferential pathway and saturated hydraulic conductivity of material filling the channel, other factors such as the geometry of the flow pathway, the geometry of the sloped cover, and the characteristics of the cover soils can all affect the final water balance components (especially the percolation to the underlying waste rock) and, consequently, the performance of the cover system during preferential flow. Further research is necessary to shed more light on the effect of preferential flow in barrier layers on the long-term performance of the soil covers.

Significance to the engineered soil cover design

Through sensitivity analysis of the location of the channel flow pathway, it was found that the sum of the percolation and interflow was relatively constant and only changed slightly when the location of the channel flow pathway changed. This phenomenon may be used to identify the position of the channel pathway developed in the barrier layer through measurement of the water balance components in the field, hence providing the possibility to locate and repair cracks that may have developed in the barrier. Water balance components, especially runoff, interflow, and percolation will change depending on the location of cracks and hence preferential flow. Of course, many other factors such as geometry and frequency of the cracks (macropores) may also influence the water balance components.

The modeled results showed that the percolation was sensitive to both the location of the channel pathway and the saturated hydraulic conductivity of material filling the channel pathway, so ideally, the best cover design should minimize the development of preferential flow in the barrier layer. In practice, however, cracks may form and compromise the performance of the cover. The sensitivity analysis also indicated that the maximum percolation occurred when the channel pathway was located downslope; therefore the soil cover design and construction should include special measures to avoid the formation of cracks and preferential flow downslope. If the generation of preferential flow were inevitable, decreasing the percolation could be an option. In the modeled cases, the actual evaporation did not change significantly with the location of the channel and change in the hydraulic conductivity of the channel material. The water was mainly redistributed between percolation and interflow; as a result, increasing the interflow could decrease the percolation into the underlying waste rock. One way of increasing interflow from the barrier includes choosing the appropriate barrier material, geometry (or topography) and configuration of the soil cover. It should be noted that forgoing analysis and discussion are based on consideration of percolation alone. Since channeling may also impact ingress of gaseous oxygen into the underlying waste rock, oxygen transfer is a factor that must be considered. Increased oxygen due to channeling can result in increased oxidation of sulfide-bearing minerals present in the waste rock. Thus, oxygen flux analysis should also be conducted in the design to minimize the effect of channeling on soil cover performance.

Conclusions

A 10-cm-wide channel pathway installed in a layered soil cover with a slope of 20% was modeled physically in the laboratory. The cover consisted of sand and silty clay overlying acid-generating waste rock. Measured water balance components were simulated with the commercial computer program, VADOSE/W. Further modeling was conducted to analyze the effects of the location of the channel pathway and the saturated hydraulic conductivity of the material filling the channel on water balance components. Based on the measurement and modeling, the following is concluded:

1. Measured matric suction in the sand layer decreased and water content increased from upslope to downslope. The silty clay layer maintained high saturation during entire the test. The volumetric water content of the waste rock obtained from TDR measurements was lower than water content obtained from oven drying. Continuous oxidation of the waste rock probably affected the TDR waveforms, resulting in the discrepancy.
2. Measured percolation in the test accounted for 43.0% of the total precipitation, interflow for 35.3% and actual evaporation for 23.6%.

3. The measured and modeled results indicated that precipitation intensity affected the maximum change in soil water storage in the cover during rainfall events. High precipitation intensity produced a large change in soil water storage during rainfall.
4. The computer program reasonably simulated the measured water balance in the experiment. A careful, step-by-step modeling approach and slight adjustment in the hydraulic conductivity-suction function of the sand layer was used to achieve a satisfactory match.
5. The modeled percolation increased almost linearly with the location of the channel from upslope to downslope when the normalized distance of the channel pathway to the highest point on the slope was less than 0.71. The maximum percolation, 80.1% of the total precipitation, was obtained when the normalized distance of the channel pathway was 0.71. Interflow decreased almost linearly with an increase in the normalized distance of the channel pathway when the normalized distance was less than 0.71. The interflow was 2.5% and zero when the normalized distance of the channel pathway was 0.71 and 0.96, respectively. The sum of percolation, interflow, and actual evaporation was relatively constant ranging from 104.0 to 106.5% when the location of the channel pathway varied.
6. When the channel pathway was located upslope with a normalized distance of 0.29 (the same as built in the experimental box), the modeled percolation increased and interflow decreased steadily with increasing saturated hydraulic conductivity of the material filling the channel, and these changes were quite significant when the saturated hydraulic conductivity of the channel material was less than twice the hydraulic conductivity of the overlying sand (24.2 m/day).
7. The modeled results indicate that percolation is sensitive to both the location of the channel pathway and the saturated hydraulic conductivity of material filling the channel, so cover design and construction should avoid producing vertical preferential flow in a barrier layer.

Acknowledgments Funding for this research has been provided by the Natural Sciences and Engineering Research Council of Canada in the form of an Individual Discovery Grant awarded to E.K.Yanful.

References

Adu-Wusu C, Yanful EK (2006) Performance of engineered test covers on acid-generating waste rock at Whistle mine, Ontario. Can Geotech J 43:1–18

Adu-Wusu C, Yanful EK (2007) Post-closure investigation of engineered test covers on acid-generating waste rock at Whistle Mine, Ontario. Can Geotech J 44:496–506

Adu-Wusu C, Yanful EK, Lanteigne L, O'Kane M (2007) Prediction of the water balance of two soil cover systems. Geotech Geol Eng 25:215–237

Akindunni FF, Gillham RW, Nicholson RV (1991) Numerical simulations to investigate moisture-retention characteristics in the design of oxygen-limiting covers for reactive mine tailings. Can Geotech J 28:446–451

Aubertin M, Bussière B (2001) Discussion of "Water flow through cover soils using modeling and experimental methods". J Geotech Geoenviron Eng 127:810–811

Beven K, Germann P (1982) Macropores and water flow in soils. Water Resour Res 18:1311–1325

Bussière B, Aubertin M, Chapuis RP (2003) The behavior of inclined covers as oxygen barriers. Can Geotech J 40:512–535

Choo L-P, Yanful EK (2000) Water flow through cover soils using modeling and experimental methods. J Geotech Geoenviron Eng 126:324–334

Corser P, Cranston M (1991) Observations on long-term performance of composite clay liners and covers. In: Proceedings on geosynthetic design and performance. 6th annual symposium. Vancouver Geotechnical Society, 24 May 1991. VGS, Vancouver, p 16

Daniel DE, Benson CH (1990) Water content-density criteria for compacted soil liners. J Geotech Eng ASCE 116:1811–1830

Edlefsen NE, Anderson ABC (1943) Thermodynamics of soil moisture. Hilgardia 15:21–298

Egiebor NO, Oni B (2007) Acid rock drainage formation and treatment: a review. Asia Pac J Chem Eng 2:47–62

Fala O, Molson J, Aubertin M, Bussière B (2005) Numerical modeling of flow and capillary barrier effects in unsaturated waste rock piles. Mine Water Environ 24:172–185

Fayer MJ (2000) UNSAT-H version 3.0: Unsaturated soil water and heat flow model, theory, user manual, and examples. Pacific Northwest national laboratory, Richland

Fredlund DG, Rahardjo H (1993) Soil mechanics for unsaturated soils. John Wiley & Sons Inc, New York

Fredlund DG, Xing A (1994) Equations for the soil-water characteristic curve. Can Geotech J 31:521–532

Fredlund DG, Xing A, Huang S (1994) Predicting the permeability function for unsaturated soils using the soil-water characteristic curve. Can Geotech J 31:533–546

GEO-SLOPE (2002) SEEP/W for finite element seepage analysis, user's guide. GEO-SLOPE International Limited, Calgary, Alberta, Canada

GEO-SLOPE (2004) VADOSE/W 2004 User's guide. GEO-SLOPE International Limited, Calgary, Alberta, Canada

Hill DE, Parlange J-Y (1972) Wetting front instability in layered soils. Soil Sci Soc Am J 36:697–702

Khire MV, Benson CH, Bosscher PJ (1999) Field data from a capillary barrier and model predictions with UNSAT-H. J Geotech Geoenviron Eng 125:518–528

Krahn J (2004) Vadose zone modeling with VADOSE/W: An engineering methodology. GEO-SLOPE International Ltd, Calgary, Alberta, Canada

Kung K-JS (1990) Preferential flow in a sandy vadose zone, 2, Mechanisms and implications. Geoderma 46:59–71

MEND (1991) Acid rock drainage prediction manual. MEND Project 1.16.1b. Coastech Research Inc., Vancouver

Mitchell JK, Hooper D, Campanella R (1965) Permeability of compacted clay. J Soil Mech Found Div Proc Am Soc Civil Eng 91:41–65

Nadler A, Gamliel A, Peretz I (1999) Practical aspects of salinity effect on TDR-measured water content: A field study. Soil Sci Soc Am J 63:1070–1076

Nichol C, Smith L, Beckie R (2003) Time domain refelectrometry measurements of water content in coarse waste rock. Can Geotech J 40:137–148

Nicholson RV, Gillham RW, Cherry JA, Reardon EJ (1989) Reduction of acid generation in mine tailings through the use of moisture-retaining cover layers as oxygen barriers. Can Geotech J 26:1–8

O'Kane M, Wilson GW, Barbour SL (1998) Instrumentation and monitoring of an engineered soil cover system for mine waste rock. Can Geotech J 35:828–846

Pham HQ, Fredlund DG, Barbour SL (2005) A study of hysteresis models for soil-water characteristic curves. Can Geotech J 42:1548–1568

Scanlon BR, Christman M, Reedy RC, Porro I, Simunek J, Flerchinger GN (2002) Intercode comparisons for simulating water balance of surficial sediments in semiarid regions. Water Resour Res 38:591–5916

Schroeder PR, Aziz NM, Lloyd CM, Zappi PA (1994) The hydrologic evaluation of landfill performance (HELP) model: user's guide for version 3. EPA/600/R-94/168a, September 1994. U.S. Environmental Protection Agency Office of Research and Development, Washington

Selker JS, Steenhuis TS, Parlange J-Y (1992) Wetting front instability in homogeneous sandy soils under continuous infiltration. Soil Sci Soc Am J 56:1346–1350

Simunek J, Sejna M, van Genuchten MTh (1999) The HYDRUS-2D software package for simulating two-dimensional movement of water, heat, and multiple solutes in variably-saturated media, version 2.0. U.S. Salinity Laboratory, USDA, ARS, Riverside

Simunek J, van Genuchten MTh, Sejna M (2005) The HYDRUS-1D software package for simulating the movement of water, heat, and multiple solutes in variably saturated media, version 3.0, HYDRUS software series 1. Department of Environmental Sciences, University of California Riverside, Riverside

Song Q, Yanful EK (2008) Monitoring and modeling of sand-bentonite cover for ARD mitigation. Water Air Soil Pollut 190:65–85

Song Q, Yanful EK (2009a) Effect of channelling on water balance, oxygen diffusion and oxidation rate in mine waste rock with an inclined multilayer soil cover. J Contam Hydrol (in final review)

Song Q, Yanful EK (2009b) Effect of water addition frequency on oxygen consumption in acid generating waste rock. Accepted for publication in ASCE J Environ Eng (in press)

Suter GW, Luxmoore RJ, Smith ED (1993) Compacted soil barriers at abandoned landfill sites are likely to fail in the long term. J Environ Qual 22:217–226

Swanson DA, Barbour SL, Wilson GW, O'Kane M (2003) Soil-atmosphere modelling of an engineered soil cover for acid generating mine waste in a humid, alpine climate. Can Geotech J 40:276–292

Taha MR, Kabir MH (2005) Tropical residual soil as compacted soil liners. Environ Geol 47:375–381

Taylor G, Spain A, Nefiodovas A, Timms G, Kuznetsov V, Benntt J (2003) Determination of the reasons for deterioration of the Rum Jungle waste rock cover. Australian Center for Mining Environmental Research, Brisbane

Topp GC, Davis JL, Annan AP (1980) Electromagnetic determination of soil water content: Measurements in coaxial transmission lines. Water Resour Res 16:574–582

van Genuchten MTh (1980) A closed-form equation for predicting the hydraulic conductivity of unsaturated soils. Soil Sci Soc Am J 44:892–898

Walter MT, Kim J-S, Steenhuis TS, Parlange J-Y, Heilig A, Braddock RD, Selker JS, Boll J (2000) Funneled flow mechanisms in a sloping layered soil: laboratory investigation. Water Resour Res 36:841–849

Wilson GW (1990) Soil evaporative fluxes for geotechnical engineering problems. Ph.D. Thesis, University of Saskatchewan, Saskatoon, Canada

Wilson GW, Fredlund DG, Barbour SL (1994) Coupled soil atmosphere modeling for soil evaporation. Can Geotech J 31:151–161

Woyshner MR, Yanful EK (1995) Modeling and field measurements of water percolation through an experimental soil cover on mine tailings. Can Geotech J 32:601–609

Yanful EK, Mousavi SM, Yang M (2003) Modeling and measurement of evaporation in moisture-retaining soil covers. Adv Environ Res 7:783–801

Yang H, Rahardjo H, Leong EC, Fredlund DG (2004) A study of infiltration on three sand capillary barriers. Can Geotech J 41:629–643